journal

Reprinted from the Journal of the American Ceramic Society, Vol. 76, No. 6, June 1991

J. Am. Ceram. Soc., 74 [6] 1340–48 (1991)

Cyclic Fatigue from Frictional Degradation at Bridging Grains in Alumina

Srinivasarao Lathabai,*[,†,‡] Jürgen Rödel,[†] and Brian R. Lawn*

Ceramics Division, National Institute of Standards and Technology, Gaithersburg, Maryland 20899

Tension–tension cyclic loading tests have been conducted on a coarse-grained alumina ceramic that exhibits toughness-curve behavior by grain-interlock bridging. Fatigue effects are observed in the regions of both short cracks, using indentation flaws, and long cracks, using compact-tension specimens. A true mechanical fatigue effect is demonstrated by running the tests below the static fatigue limit. A custom-made device for in situ observation of crack propagation in the scanning electron microscope enables us to identify bridge degradation as a cause of the fatigue process. "Wear" debris cumulates at the sliding intergranular frictional contact points, indicating a loss of traction at the junction. The basis of a fracture mechanics model describing the effect of this frictional degradation in reducing crack-tip shielding is outlined and fitted to the data. It is suggested that the bridge degradation fatigue mechanism may be widespread in polycrystalline ceramics with pronounced toughness curves. [Key words: fatigue, friction, degradation, grains, bridging.]

I. Introduction

A NEW breed of flaw-tolerant ceramics is emerging. Flaw tolerance is a manifestation of crack-tip shielding that cumulatively toughens the material as the crack extends, resulting in an increasing toughness curve (*R*-curve or *T*-curve).[1] Several shielding processes have been considered in the literature, most notably frontal-zone phase transformation and microcracking. But in monophase ceramics like aluminas the principal mode is bridging of the crack interface by interlocking grains.[2–4] A leading question in the potential use of such materials for structural applications is whether the elements responsible for the toughening degrade during reversed loading: do bridging materials exhibit true, mechanical cyclic fatigue, and, if so, what is the degradation mechanism?

Early studies on alumina[5–8] reported reduced lifetimes in cyclic relative to static loading. A fracture mechanics analysis of results on glass and porcelain (in the context of a review of some of the earlier data[5,8]) suggested that the fatigue could be explained as the integrated effect of environmentally enhanced slow crack growth.[9] A study on silicon carbide[10] showed no cyclic effect at all. However, more recent studies on aluminas,[11,12] zirconias,[13,14] silicon nitrides,[15–20] and fiber-reinforced ceramics[21] do appear to demonstrate definite mechanical cyclic fatigue.

If authentication of the *existence* of true cyclic fatigue has been slow in coming, identification of the responsible mechanisms of degradation is virtually *totally* lacking. Some authors, drawing largely from the greater knowledge of fatigue processes in metallic materials, have proposed very specific mechanisms for fatigue damage in ceramics.[22–24] One class of these mechanisms invokes crack "closure,"[§] including wedging by crack-interface asperities, debris, and the like; others invoke frontal-zone microcracking or even microplasticity. However, direct experimental evidence proving or disproving these hypothetical mechanisms is lacking. The possibility of interfacial bridge degradation has hardly been given any consideration at all in the literature.[21,25]

Our objective in the present study is to investigate the effect of cyclic tension–tension loading on an alumina ceramic with a demonstrably pronounced *T*-curve from bridging, in the opposite domains of "short" cracks pertinent to strength properties and "long" cracks encountered in specimens for toughness evaluations. For the short cracks we use indentation flaws, comparing lifetimes of flexure specimens under cyclic loading with those of control static specimens. In an earlier, less complete study of this kind in our laboratories[26] on a finer-grained alumina (i.e., with weaker *T*-curve) we were unable to detect any true degradation, over and above that due to moisture-induced slow growth, in the strength properties. For the long cracks we use a compact-tension geometry, subjecting the specimen to cyclic loading at various interruption stages in the crack extension. Evidence for modest mechanically induced cyclic fatigue is found in both crack-size domains.

In light of the hypothetical nature of previously proposed fatigue mechanisms, we use a custom-designed device[27,28] for in situ viewing of cracks in our material in the scanning electron microscope (SEM). *Direct observations during cyclic loading reveal the cumulation of debris at sliding grain facets along the crack interfaces.* A specific model for fatigue damage in bridging ceramics, based on frictional degradation at grain-interlock "pullout" sites, is thereby advanced. It is proposed that frictional degradation may be a dominant fatigue mechanism in a broad range of ordinary monophase and multiphase ceramics, and therefore a factor for special consideration in designing with such materials.

II. Experiment

The material used in this study was a commercial polycrystalline alumina, with <0.1% additive.[¶] The specimens were obtained as disks 22 mm in diameter and 2 mm thick, and plates 100 mm × 100 mm × 6 mm. This alumina was nominally the same as used in our earlier study,[26] except that it was subjected to a heat treatment to coarsen the mean grain size, from 23 to 35 μm, and thereby to strengthen the *T*-curve. It fractured predominantly by intergranular fracture, with some

K. Faber—contributing editor

Manuscript No. 197256. Received October 1, 1990; approved March 11, 1991.

Presented at the 92nd Annual Meeting of the American Ceramic Society, Dallas, TX, April 25, 1990 (Paper No. J-XX-90).

Supported by the U.S. Air Force Office of Scientific Research.

*Member, American Ceramic Society.

†Guest scientist from the Department of Materials Science and Engineering, Lehigh University, Bethlehem, PA.

‡Now in the Division of Materials Science, CSIRO, Clayton, Victoria 3168, Australia.

§A term coined by metallurgists to designate a residual *opening* on unloading.

¶Vistal grade Al_2O_3, Coors Ceramics Co., Golden, CO.

transgranular fracture through the larger grains.[2,4] Fatigue tests were run in tension–tension loading, as follows.

(1) Short-Crack Fatigue Tests

"Short-crack" tests were conducted on the disks. Vickers indentation flaws at a load of 30 N (immediate postcontact radial crack dimension ≈100 μm) were placed at the centers of the prospective tensile faces. The indented disks were mounted on a biaxial loading fixture,[29] using a flat circular punch of diameter 4 mm on a three-point support of diameter 19 mm. Cyclic tests were run in water, with sinusoidal loading at frequencies of 1 and 100 Hz on a digitally controlled servo-hydraulic testing machine.[††] The maximum tensile stress was adjusted as required, but the minimum was maintained constant at 20 MPa. Runs were discontinued if no failure occurred within 24 to 40 h. Control tests were carried out under static loading in water, at the same maximum levels as in the cyclic runs. Additional, "calibration" strength tests were run at the same indent load (30 N) at constant stressing rates in water, and at various loads in inert environment (silicone oil), to evaluate the intrinsic crack velocity and microstructural T-curve parameters for our material.[30]

(2) Long-Crack Fatigue Tests

"Long-crack" tests were conducted on two plate specimens, width 44 mm (measured from the load line), in the compact-tension geometry of ASTM E399.[31] The viewing surfaces of these specimens were polished to 1-μm finish, for optimal crack observation. A starter notch of length 14 mm and tip radius ≈420 μm was machined into each specimen. To control pop-in, a half-chevron slot of included angle ≈28° and radius ≈200 μm was sawn at the end of the machined notch, so that the slot extended just beyond the notch on the polished surface. A Vickers indentation (50 N) was placed ≈200 μm in front of the half-chevron on this latter surface. This led to a precrack of length ≈250 μm on loading. After subsequent incremental extensions the crack was resawn to within ≈300 μm of the new crack tip.

One of the specimens was then loaded in displacement-control mode in the servo-hydraulic testing machine, in laboratory atmosphere (relative humidity 50% to 60%). A traveling microscope was used to track the crack growth. At the first sign of slow crack growth the crack was immediately unloaded, to avoid premature failure of the system. The specimen was then transferred to a transmission optical microscope, and the crack length measured. A crack-opening-displacement (COD) gauge attached to the crack notch mouth (via steel knife edges fixed to the specimen with epoxy) enabled the load at which crack growth initiated to be readily determined as the point where the load–displacement record deviates from linearity. The applied stress-intensity factor K_A at each such point of crack growth was computed from the ASTM standard formula.[31] This procedure was repeated at various crack growth increments in monotonic loading, to allow for determination of the quasi-static toughness curve as a function of crack extension, $K_A(\Delta c) = T(\Delta c)$.[1]

A similar procedure was adopted for the second specimen, except that now the specimen was only partially unloaded at the interruption points, and then subjected to a specified static-cyclic loading sequence. Static loading was thus run at a stress-intensity factor $K_A = 0.8$ to 0.9 times that for quasi-static extension in monotonic loading. Cyclic loading was sinusoidal, frequency 10 Hz, at maximum $K_A^{Max} = K_A$ and amplitude $K_A^{Min}/K_A^{Max} = 0.1$. In these experiments the crack length was carefully monitored via the traveling microscope, and the system once more unloaded after extensions of 500 μm or more. After each such interval of static-cyclic loading the crack was reloaded to quasi-static extension and the toughness reevaluated.

[††]Instron Digital Servo-hydraulic Testing Machine 8502, Instron Corp., Canton, MA.

(3) In Situ Observations of Bridging Crack

In situ fatigue tests were conducted using a custom-designed device for incorporation in the SEM,[27,28] similar in design to that of Frei and Grathwohl.[25] Compact-tension specimens were prepared as above for the SEM in situ observations, except that the cracks were always contained within the initial chevron sawcut as an extra precaution against uncontrolled crack instability.[27] At the vacuum level in the SEM environmentally induced slow crack growth was almost totally eliminated, although some was occasionally observed if this vacuum was allowed to deteriorate (e.g., after switching off the diffusion pump). The viewing surfaces were again polished to 1-μm finish, and gold coated before insertion into the SEM. After the crack was propagated to a suitable crack length, the opening force was reduced to a level $K_A = 0.8T$ to $0.9T$ (T the toughness at that length in monotonic loading) and the specimen subjected to an interval of cycling. This was done via a piezoelectric drive controlled remotely through a function generator outside the SEM chamber.[27,28] The frequency was limited to a maximum of 2 Hz. The load amplitude was also limited, thereby necessitating manual preload of the crack before insertion into the SEM. Several locations of interest along the crack interface could be monitored during the cycling interval by means of a videocassette recorder, and photographed at static load at any point.

III. Results

(1) Short-Crack Fatigue Tests

The lifetime data for the indentation-flaw specimens are summarized in Figs. 1 to 3. Figure 1 shows the time to failure at static stresses, σ_A = constant. "Survivors" are represented by arrows. We note that the lifetime varies dramatically with minute changes in the applied stress, indicating that the system is close to a static fatigue limit for this material: i.e., the cracks are growing close to a threshold in the intrinsic crack velocity function.[30] Thus by operating at this stress level we may conveniently minimize the role of chemically assisted slow growth in the cyclic tests. The curve through the data represents a theoretical prediction (Section IV) from the calibrated microstructural T-curve and crack velocity parameters at the prescribed indentation load.[26,30]

Figure 2 shows the comparative lifetime data for cyclic loading as a function of maximum applied stress, σ_{Max}, at the two frequencies used. A rapid variation of lifetime with applied stress is again apparent, although in this case there does appear to be some indication of a systematic if modest falloff relative to the predicted curves for kinetic crack growth

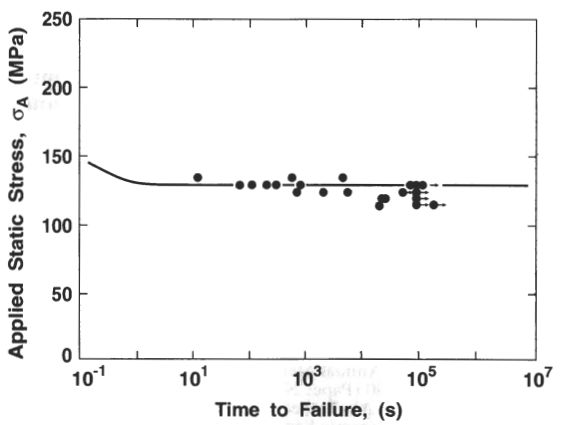

Fig. 1. Lifetimes in static loading of alumina in water, Vickers indentations (P = 30 N). Most data points are results of individual tests; those with arrows are means of interrupted tests for a minimum of five specimens. Solid curve is theoretical prediction. Note fatigue limit.

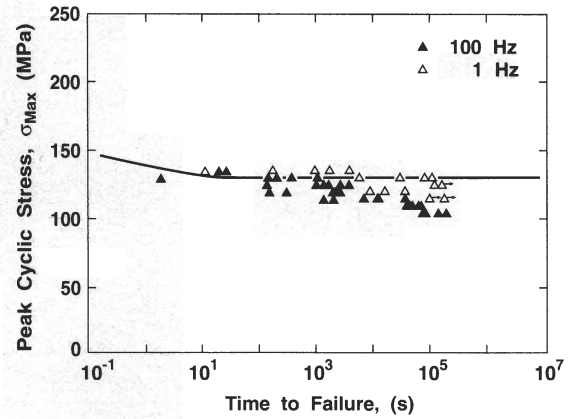

Fig. 2. Lifetimes in cyclic loading of alumina in water, Vickers indentations (P = 30 N). Data points are individual tests, open symbols 1 Hz, closed symbols 100 Hz; arrows are interrupted tests, minimum of five specimens. Solid line is theoretical prediction assuming environmentally-assisted slow crack growth without mechanical degradation.

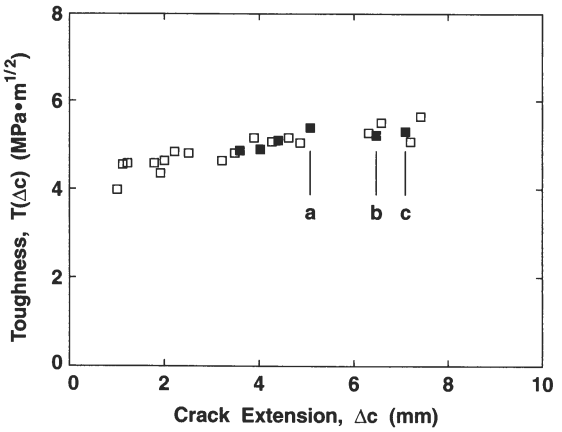

Fig. 4. Toughness curves for two alumina compact-tension specimens (distinguished by open and closed symbols) in air. Unlabeled points represent quasi-equilibrium crack extension in monotonic loading. Labeled points a, b, c represent similar extension but after interruption static-cyclic sequence (see Fig. 5 for details).

alone,[26] especially at the higher frequency. The falloff is seen to better effect in Fig. 3, which replots the data as a function of cycles to failure. The fact that the data fit a more universal curve in the replotted figure is further indication that the fatigue is due to a true mechanical effect.

(2) Long-Crack Fatigue Tests

Results of the compact-tension toughness-curve tests are plotted in Fig. 4. Data for the two specimens overlap within experimental error, saturating at $T \approx 5.3$ MPa·m$^{1/2}$. We reemphasize that the toughness values in this plot are quasi-static, in that the tests are carried out in air and the crack does not extend in strict equilibrium; i.e., the configuration is located partway up the velocity curve in monotonic loading. Recalling that one of these specimens was subjected to interrupted static and cycling sequences, we conclude that any degradation of the shielding that might have occurred in reversed loading is insufficient, at least over the cyclic range covered, to be detectable in the toughness data.

At the same time, there is compelling evidence, from the measurements of crack extensions δc over the interruption intervals δt, that some such degradation *does* occur. The results of three interrupt sequences, each at specified values of K_A(static) = K_A^{Max}(cyclic), are plotted in Fig. 5. In each case $\delta c/\delta t$ is significantly larger in cyclic relative to static loading, despite the smaller time-averaged K-field. Note in particular the first two sequences at K_A = 4.2 MPa·m$^{1/2}$ (i.e., at 0.8T): there is a total absence of crack growth in the static phase, indicating that at this K_A level the system lies below the crack velocity threshold; and yet there is significant extension in the ensuing cyclic phase, again implying some mechanical fatigue effect.

(3) In Situ Observations

The in situ SEM device provided an opportunity to follow the development of bridging sites along the intergranular crack interface during cyclic loading tests. Notwithstanding the practical limitation on number of cycles, evidence for continuing bridge evolution was obtained in these tests, with and without attendant crack propagation. Selected sequences are shown in Figs. 6 to 10 (crack propagation top to bottom and applied loading horizontal in all cases). All bridging elements in these sequences are photographed at peak crack opening in the in situ cycle unless otherwise qualified, with number of cycles n and distance x behind crack tip indicated where appropriate:

(i) Figure 6: Segmentation of a bridging grain at three stages in its development. Between (a) and (b), after a few thousand cycles and minor crack propagation, the crack closes at lower right (segment P) and redirects, releasing internal stress in the intervening grain.[27] Between (b) and (c), the crack propagates further by virtue of an increment in the applied load, and undergoes a further closure relaxation at upper right (segment Q). This example demonstrates the general

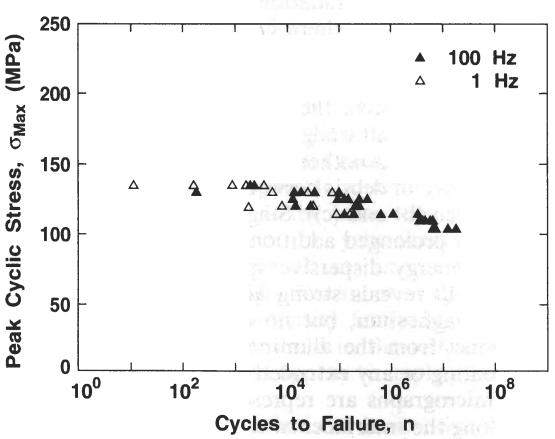

Fig. 3. Replot of data in Fig. 2 as function of cycles to failure. Symbols as in Fig. 2.

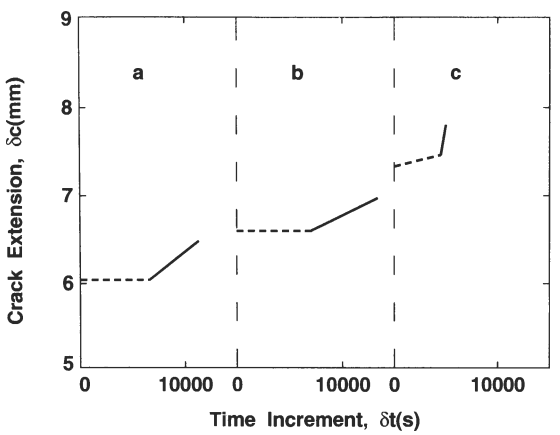

Fig. 5. Crack extensions during intervals in static-cyclic (10 Hz) interruption sequences at points labeled in Fig. 4. Measurements of c and t were made at end points of each straight line segment, so slopes are average velocities: (a) $K_A = K_A^{Max}$ = 4.2 MPa·m^{12}; (b) same; (c) $K_A = K_A^{Max}$ = 4.75 MPa·m$^{1/2}$.

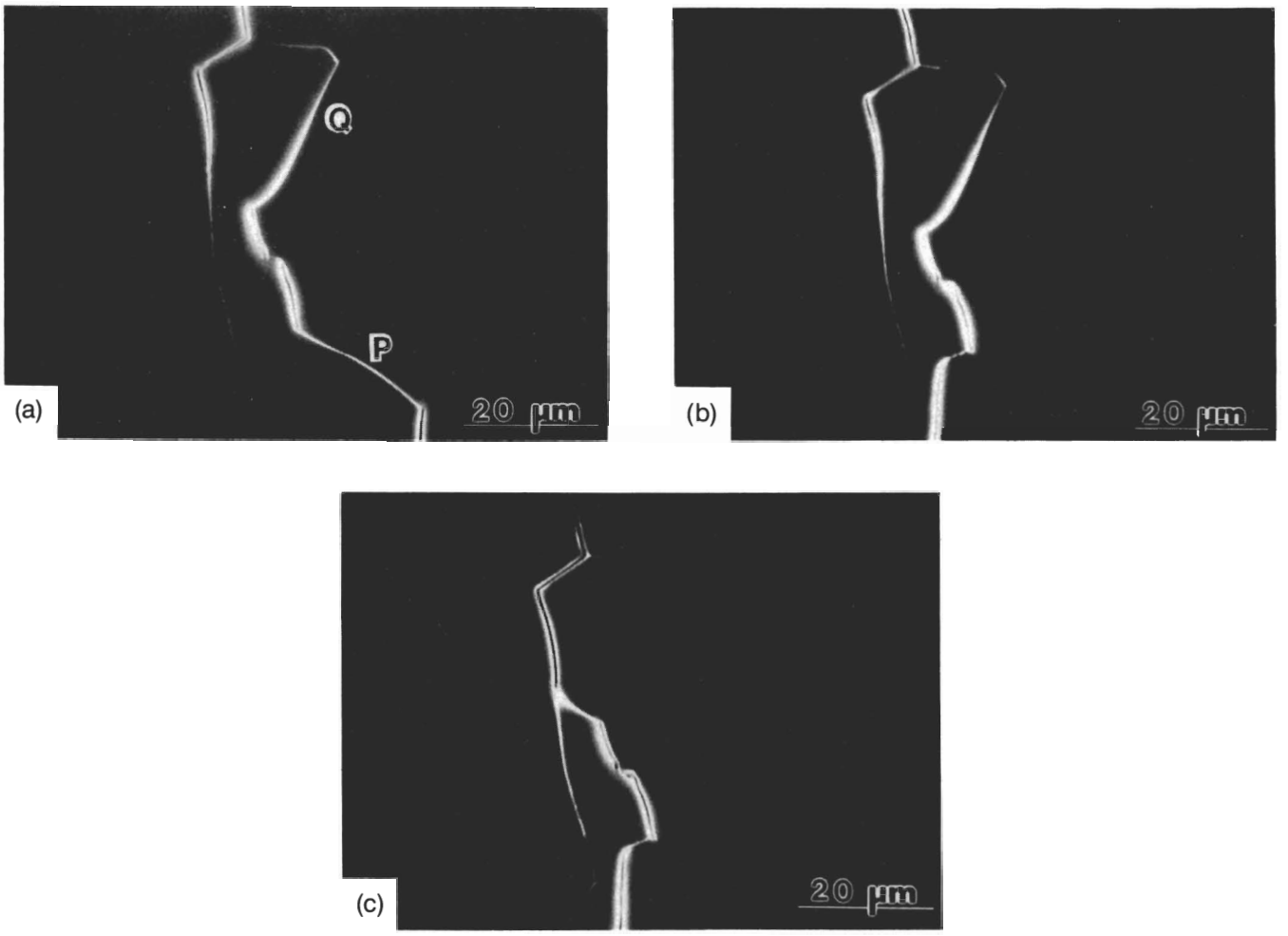

Fig. 6. SEM micrograph of crack in alumina, showing grain-bridging element: (a) after initial crack propagation (distance x = 860 μm behind crack tip); (b) after cycling in SEM (n = 7000 at 2 Hz, $K_A^{Max} = 0.85T$) and minor crack propagation (x = 880 μm); (c) after increasing K_A and further propagation (x = 1080 μm).

capacity of bridging sites to continue their evolution in response to load perturbations well after passage of the primary crack front.

(ii) Figure 7: Surface grain dislodgement from frictional rotation. Between (a) and (b) the primary crack advances under load and intergranular facet cracks link at the interlocking site, rotating the grain out of its "socket." On unloading, partially in (c) and almost completely in (d), the walls close but the grain protrudes from the surface. Note in (d) that the opening is small, ≈0.1 times that at full load in (b) (i.e., in proportion to the reduction in K_A), indicating that despite the grain dislodgement there is very little residual crack-interface wedging.

These first two sequences show distinctive evidence of bridge evolution in cyclic loading, but do not unequivocally establish a true mechanical degradation effect: how much of the evolution is due to inadvertent crack propagation, however small, during the cycling? Accordingly, the next sequences contain stages in which no propagation is observed during the cycling, and yet bridge degradation is still evident:

(iii) Figure 8: Sliding grain boundary facet with apparently strong frictional traction. Cycling between (a) and (b) produces a secondary crack below the bridging grain (P), *without detectable crack propagation.* After further loading and propagation to (c), both primary and secondary cracks open up (the former almost to the point of disengagement of the sliding grain boundary facet). Subsequent static loading at constant load in a degraded SEM vacuum (by switching off the diffusion pump overnight) causes the crack to more than double its length, disengaging the bridging grain facet totally in (d). We note the "flipover" of grain segment P from the right side of the interface to the left between (c) and (d) at the point of disengagement, suggesting that this segment remains permanently attached at its subsurface base to the left wall throughout the separation, like a highly sprung cantilever. The consequent release of elastic strain energy at disengagement in this case must be considerable and highly dissipative.

The following two sequences are further examples of bridge evolution in reversed loading, but with closer attention to degradation of frictional facets for extended cycling periods:

(iv) Figure 9: Degradation of frictional facet. Through cycling stages (a) to (e) there is gradual cumulation of debris from the sliding grain facet interface, even between (c) and (e), where no primary crack propagation occurs. Stage (f) is after total unload; note the residual opening at upper right, indicating some small wedging in this region.

(v) Figure 10: Another frictional facet. Similar to Fig. 9, with appearance of debris between (a) and (c) (no crack propagation between (b) and (c)). Stage (d) shows enhanced debris buildup after prolonged additional cycling *in air.*

Selective energy dispersive spectroscopy of the debris in Figs. 9 and 10 reveals strong aluminum and oxygen peaks, and trace magnesium, but no excess gold, consistent with some product from the alumina itself rather than from the surface coating or any extruded grain boundary phase.

These micrographs are representative of extensive examinations along the interfaces of three alumina specimens. The geometrical disposition of the interlocking configurations and

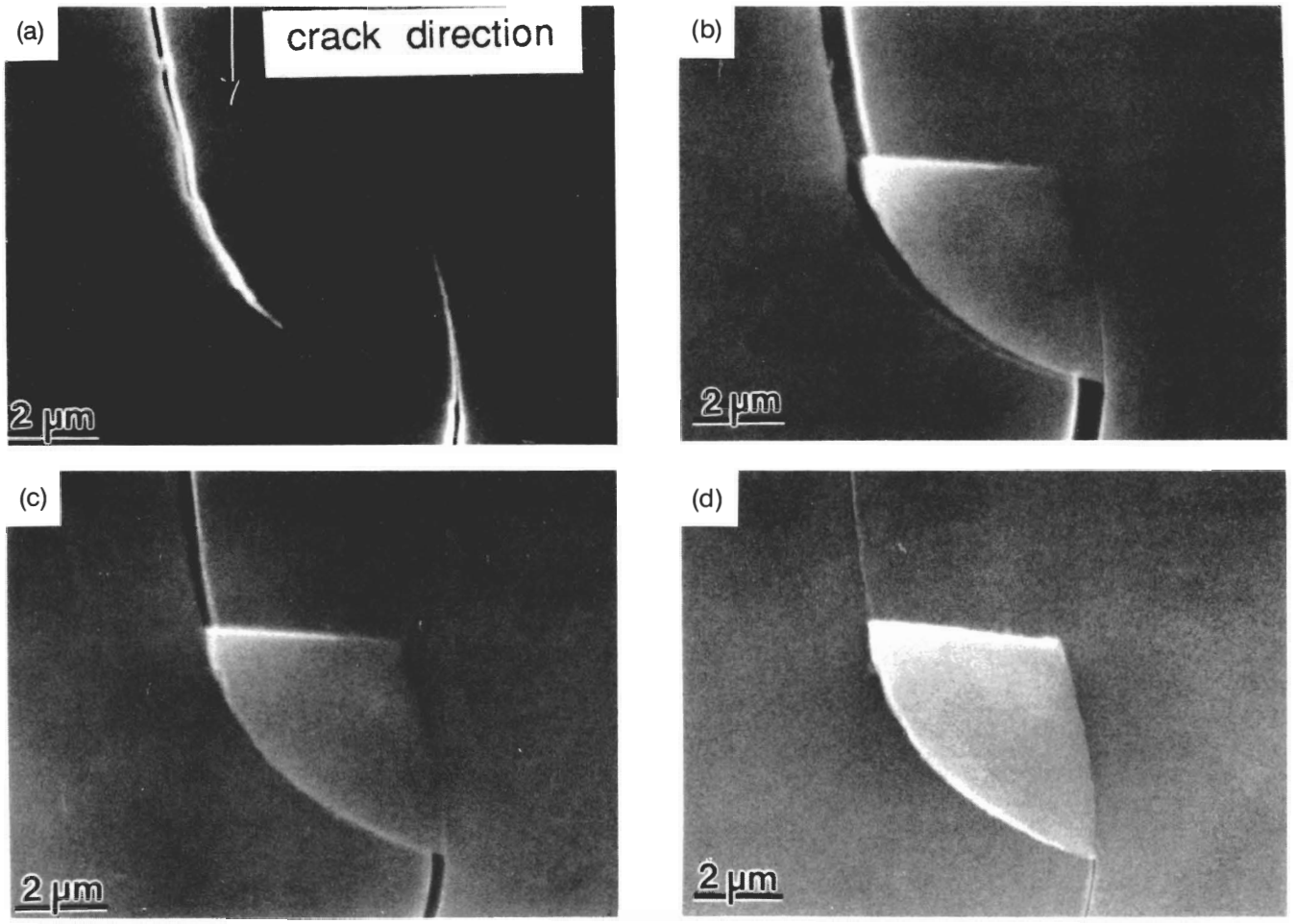

Fig. 7. SEM micrographs of grain facet: (a) after initial crack propagation (x = 170 μm), showing bridge; (b) after further loading and cycling (n = 7200 at 2 Hz, $K_A^{Max} = 0.8T$), with attendant propagation (x = 740 μm); (c) after partial unload to $K_A = 0.6T$; (d) at near-complete unload, $K_A = 0.1T$. Note near dislodgement of grain.

the associated frictional degradation varies considerably from point to point. We have given some indication of wedging at incompletely closed cracks, but this was never a large effect (residual opening always <0.2 that at full load).

As in earlier studies,[2,27] we find no evidence for detached frontal-zone microcrack clouds.

IV. Model

We noted from comparison of the indentation-strength data in Figs. 2 and 3 that it is the total number of cycles, rather than integrated time, that is the important independent variable in the lifetime characteristics. The reduction in strength of the specimens is modest, <20% in 10^6 cycles. In this context we may recall the apparent absence of any such effect in our earlier, preliminary study;[26] here we are using an alumina with a larger grain size, hence more pronounced toughness curve, and have extended the data range. Although there was little indication of any comparable reduction in toughness in the long-crack data of Fig. 4, the same tests revealed an enhancement in crack extension in cyclic loading, Fig. 5. The apparent absence of fatigue effects in control static tests (Figs. 1 and 5) is especially pertinent, implying that the (shielded) crack-tip stress-intensity factor K_* in those cases must remain below the threshold in the v–K_* curve. Taken together, these results would appear to imply a buildup of K_* during cyclic loading.

Several hypothetical mechanisms have been proposed to account for mechanical fatigue in cyclic loading. All may operate in certain materials under certain conditions, but none have hitherto been directly confirmed. In the present study we may immediately eliminate potential contributions from frontal zones,[13,14] because our material is nontransforming and we see no microcracking clouds. Geometrical processes like asperity-induced secondary cracking,[22] and wedging by debris[22,24,32] and surface roughness[22,24] ("closure"), have also been proposed; and we do see minor secondary cracking and residual crack openings at our crack interfaces. However, whereas some of these mechanisms do allow for an increase in the *mean* crack-tip stress-intensity factor K_* in cyclic loading, none allows for an enhancement in the *maximum* K_*,[24] as is necessary if the crack system is ever to rise above the velocity threshold.

The above SEM observations of frictional bridge activity suggest that the fatigue results may be due to a progressive degradation of the shielding stress-intensity factor. To quantify this, we begin by summarizing the more important elements of the toughness curve (T-curve) theory by grain-interlock bridging, referring the reader to earlier sources[26,30] for greater detail. The crack-tip stress-intensity factor is

$$K_*(c) = K_A(c) + K_R(c) + K_\mu(c) \quad (1)$$

with $K_A(c) = \psi\sigma_A c^{1/2}$ from the applied stress (ψ a geometry term), $K_R(c) = \chi P/c^{3/2}$ from any residual contact stresses (here relevant only to indentation cracks, χ a contact coefficient[1,4,30]), and $-K_\mu(c)$ a microstructural shielding term (note $K_\mu < 0$) from the bridging. This last term is a function of several microstructural parameters, among them the coeffi-

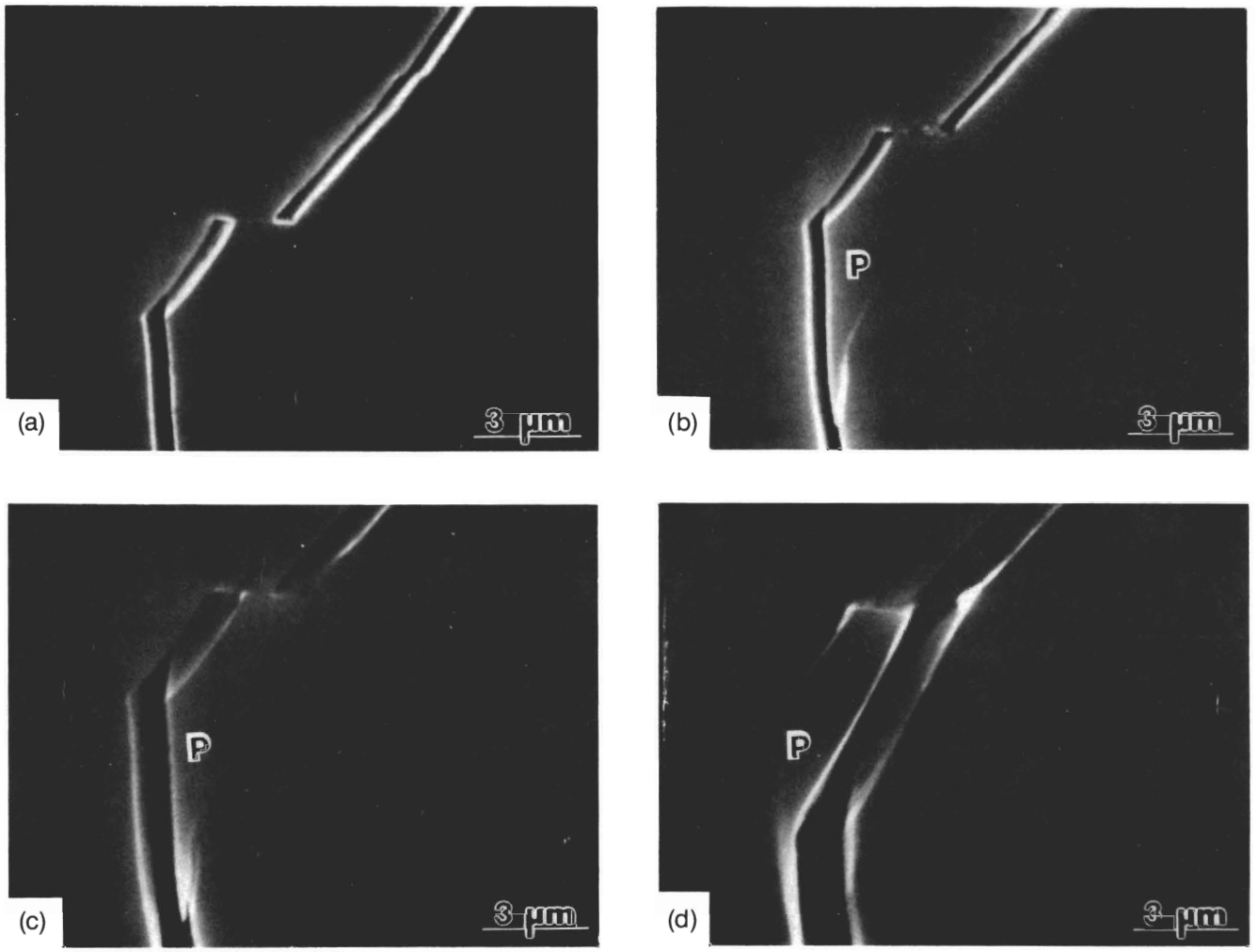

Fig. 8. SEM micrographs of frictional grain facet: (a) after initial crack propagation (x = 290 μm); (b) after cycling (n = 7200 at 2 Hz, $K_A^{Max} = 0.8T$), with no propagation; (c) after loading and cycling (n = 54000 at 2 Hz, $K_A^{Max} = 0.9T$), with accompanying propagation (x = 850 μm); (d) after static loading in degraded SEM vacuum for 16 h at $K_A = 0.9T$, with further propagation (x = 2120 μm). Note appearance of secondary crack at segment P in (b) as result of cycling only, and ultimate "flip" of this segment from right to left side of interface between (c) and (d).

cient of friction μ, between sliding facets at grain interlock sites, i.e., $K_\mu = K_\mu(\mu, c)$.[4,30] As indicated earlier, these microstructural parameters (and thence the T-curve) are calibrated from control indentation strength vs load data on our material in inert environments (Section II(1)). To accommodate environmentally-assisted slow crack growth we define a velocity function, based on thermal activation over atomically localized energy barriers[33]

$$v(G_\bullet) = v_0 \sinh [(G_\bullet - W_{BEB})/2\Gamma] \quad (W_{BEB} \le G_\bullet \le W_{BB}) \tag{2}$$

with a threshold ($v = 0$) at $G_\bullet = K_\bullet^2(1 - \nu^2)/E = W_{BEB}$: E denotes Young's modulus, ν is Poisson's ratio, and W_{BB} and W_{BEB} are the reversible work to separate the grain boundary B–B under vacuum and in environmental species E, respectively. The adjustable parameters v_0 and Γ are calibrated from strength data in water at constant stressing rates (Section II(1)). Equations (1) and (2) constitute the underlying basis of the theoretically generated plots for the appropriate stress vs lifetime functions in Figs. 1 and 2.[26]

We propose that bridge degradation with increasing cycles is manifested primarily as a progressive reduction in the friction coefficient $\mu(n)$, hence in the magnitude of the shielding term $-K_\mu(n)$. Now for any given crack length c and applied stress σ_A we have $\Delta K_\bullet = \Delta K_\mu$ from Eq. (1). Then, since $K_\mu < 0$ for bridging, we see that reduced shielding corresponds to increased $K_\bullet(n)$, in the manner of Fig. 11. Figure 12 is a plot of $\mu(n)$ corresponding to the indentation cyclic data, obtained by treating μ as an adjustable parameter and using a numerical algorithm to solve Eqs. (1) and (2) for a best fit at each point in Fig. 3.[26] We note that the reduction in μ required to explain the strength degradation is not large, i.e., <25% over the cycle range.

Using a smoothed function through the $\mu(n)$ data in Fig. 12, we may now calculate $K_\mu(n)$ from Eqs. (1) and (2) for cyclic loading in long cracks, and thence attempt to explain the data in Figs. 4 and 5. Accordingly, in Fig. 13 we plot $-K_\mu(n)$ for the loading conditions pertaining to Figs. 5(a) and (b) (i.e., no static growth). The peak crack-tip field $K_\bullet^{Max}(n)$, although starting below the threshold at W_{BEB}, attains this level after a critical interval, after which environmentally assisted slow crack growth can occur, consistent with the observations of nonzero $\delta c/\delta t$ during the cyclic loading stages in Fig. 5. At the same time, the decrement $\Delta K_\mu(n) = K_\mu(1) - K_\mu(n)$ is sufficiently small, <0.25 MPa·m$^{1/2}$, over 150 000 cycles as to pass unnoticed at the interruption points in the T-curve plots in Fig. 4.

V. Discussion

We have observed cyclic fatigue in an alumina ceramic which exhibits toughness-curve behavior by bridging. By

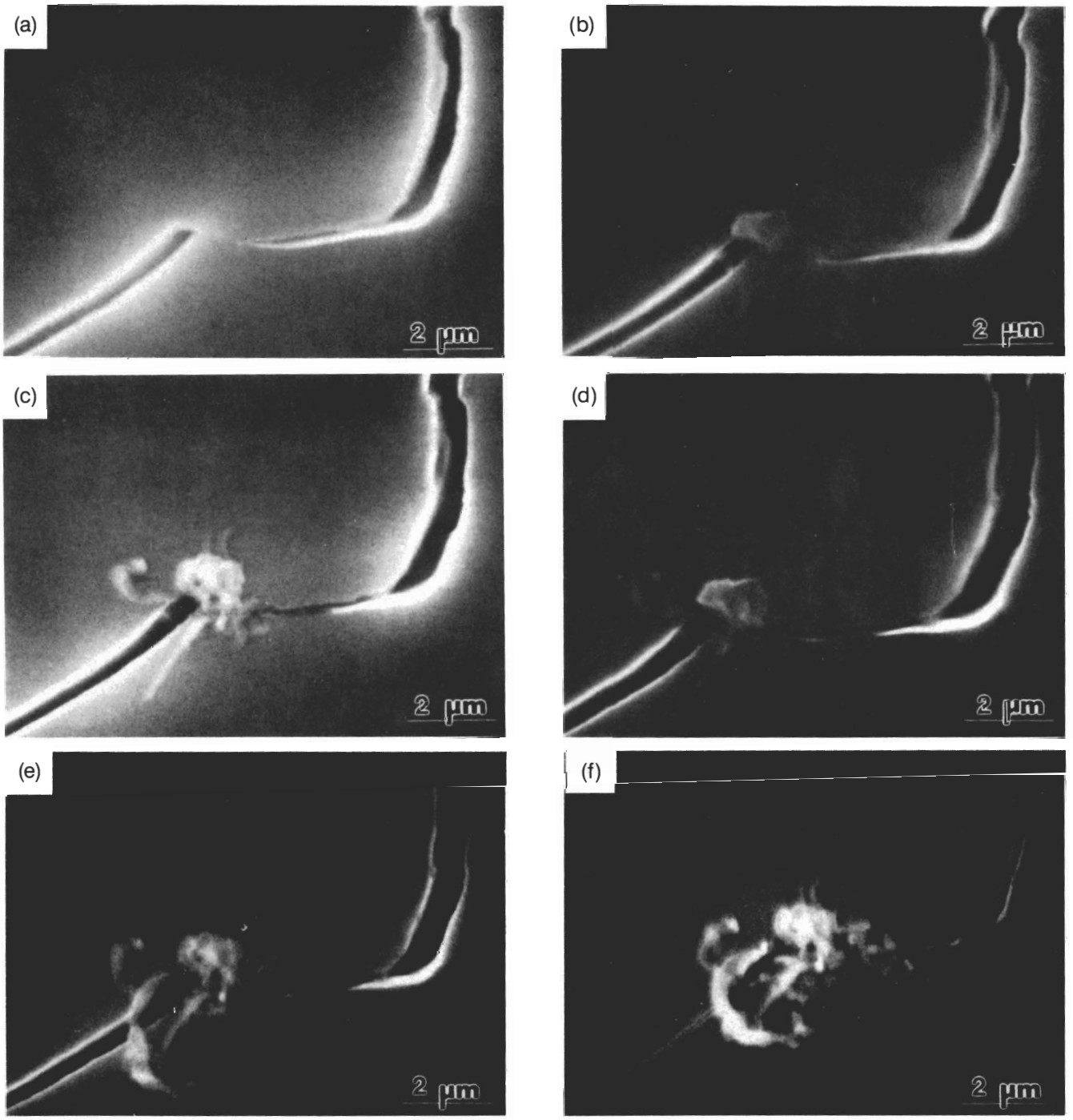

Fig. 9. SEM micrographs of frictional grain facet at various stages of cycling (all cycles at 2 Hz, $K_A^{Max} = 0.85T$): (a) after initial crack propagation (x = 610 μm); (b) after n = 7000, with minor propagation (x = 630 μm); (c) at n = 20000 and additional propagation (x = 700 μm); (d) at n = 27000, no propagation; (e) after n = 45000, no propagation; (f) total unload. Note cumulation of frictional debris at facet.

working below the static fatigue limit, i.e., below the crack velocity threshold, we are able to attribute the fatigue to true mechanical degradation of the material. On the basis of in situ observations of cracks during cyclic loading, we have proposed a new model for this degradation. Grain-interlock bridges that impart toughness can degrade in repeated unloading and reloading. The cumulation of "wear" debris at bridging sites suggests a specific mechanism of this degradation, whereby frictional tractions at sliding bridging grain boundary facets diminish progressively by persistent reversed sliding.

Notwithstanding the SEM observations, our model of a degraded frictional junction must be recognized as largely phenomenological. There are some important questions that need to be answered if we are to obtain a proper understanding of the degradation process. Thus, what is the specific nature of the friction at the intergranular sliding interface? We note that the friction coefficient is of order unity in Fig. 12, not unusual for virgin interfaces in their pristine state.[34] What is the role of environment, particularly water, in this friction? There is evidence in the wear literature that the friction at contacting surfaces of alumina can indeed be modified by repeated sliding and, moreover, that this sliding produces debris from chemical reaction with environmental species.[35] Thus interfacial friction is a vital factor not only in toughness,[4,36] but also in lifetime.

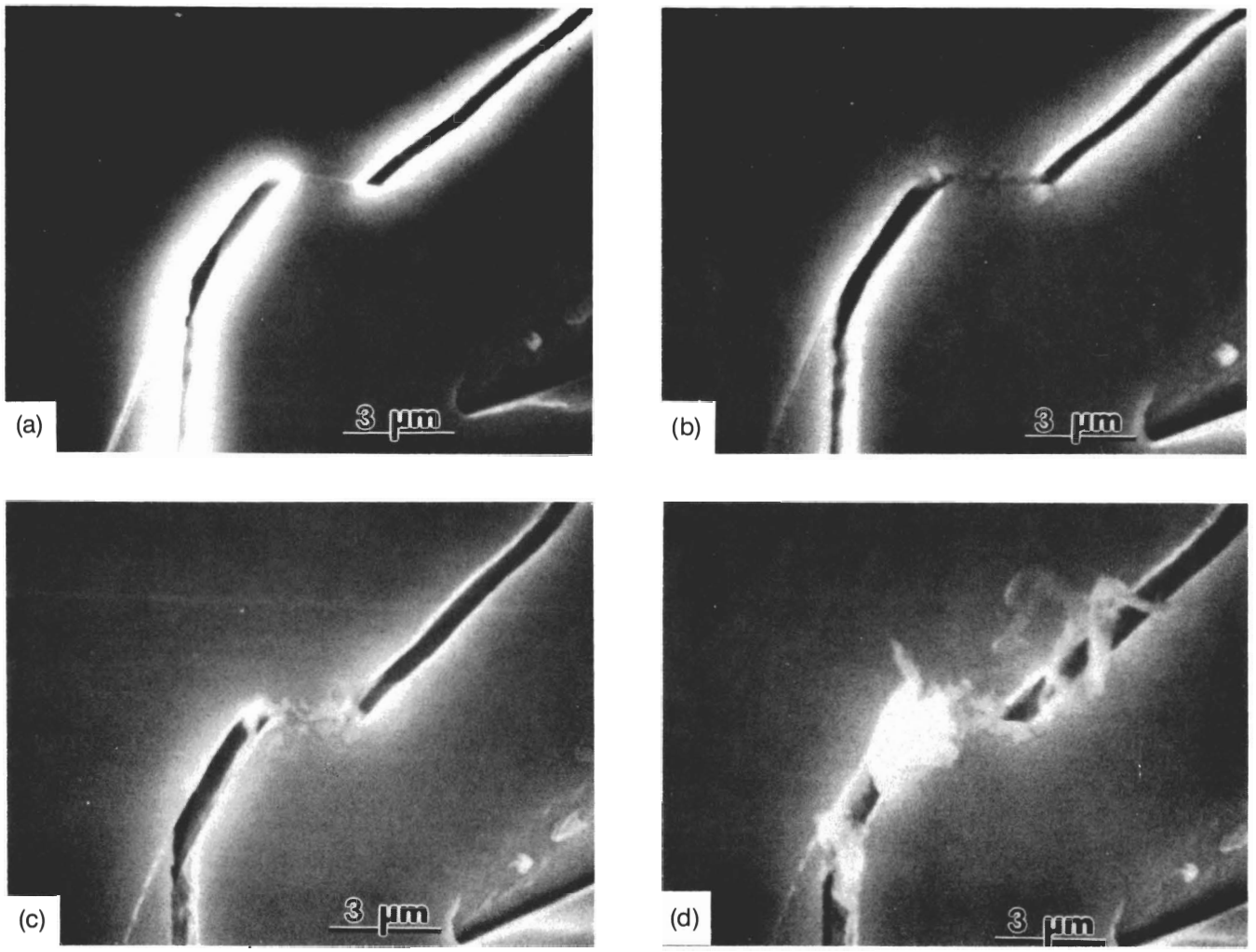

Fig. 10. SEM micrographs of another frictional grain facet at various stages of cycling (all cycles at $K_A^{Max} = 0.85T$): (a) after initial propagation (x = 820 μm); (b) after n = 20000 (2 Hz), crack propagation (x = 910 μm); (c) after n = 45000 (2 Hz), no propagation; (d) after n = 50000 (10 Hz) in air, minor propagation (x = 930 μm). Note debris.

The present study should be seen as a first step in identifying and modeling the mechanisms of cyclic fatigue in ceramics. The following aspects of the fatigue characterization warrant comment:

(i) *Generality of Model.* The indication is that our model, although formulated specifically from observations on alumina, may apply to nontransforming, bridging ceramics in general. Materials with more pronounced T-curves may therefore serve as better candidates for quantifying the degradation. There is a need to rationalize the interrelations between short- and long-crack data; thus, a null effect in one test (e.g., Fig. 4) does not necessarily translate into a null effect in another (cf. Figs. 3 and 5), making general conclusions and extrapolations suspect in the absence of a proper degradation model.

(ii) *In Situ SEM.* Direct observations are a crucial element of any proper identification of the fatigue processes in ce-

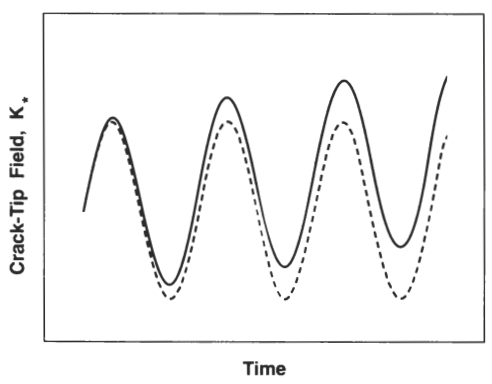

Fig. 11. Schematic illustrating possible cyclic fatigue mechanism due to frictional degradation of bridges. As shielding term diminishes with cycling, crack-tip K_* steadily increases (solid curve), until sufficient to take system above threshold on velocity curve.

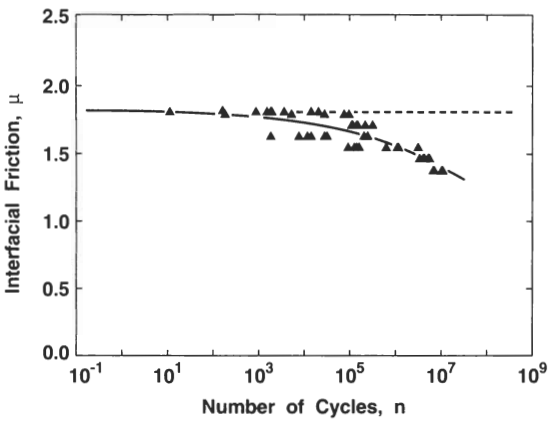

Fig. 12. Computed degradation of friction coefficient with number of cycles required to account for fatigue effect in data for alumina in Fig. 3. Dashed line is calibrated friction coefficient for monotonic loading.

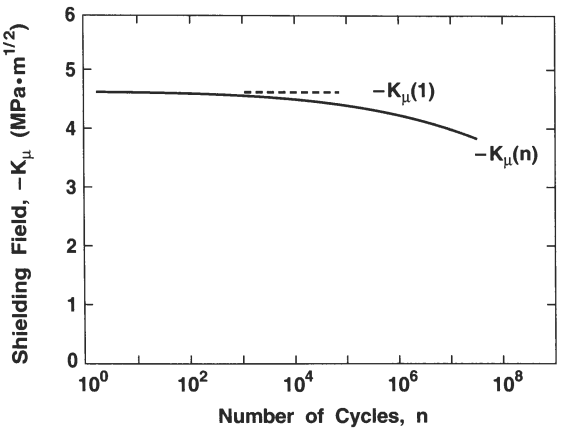

Fig. 13. Plot predicting decreasing bridging field, $-K_\mu(n)$, for cyclic loading in alumina.

ramic microstructures. This will inevitably be so in the more complex, multiphase ceramic composites, where multiple mechanisms may operate.

(iii) *Modeling.* With more positive confirmation of friction as the major microstructural variable in the degradation mechanism of cyclic fatigue, one might aim to express the model more closely in terms of documented frictional properties of interfaces, especially in regard to environmental interactions. This would open up the possibility of predetermining fatigue characteristics and tailoring interfaces for optimal resistance to degradation.

Finally, it is apparent that cyclic fatigue becomes an important design consideration in any application with moving ceramic parts. Such design will inevitably involve trade-offs. On the one hand, strong shielding is needed to promote flaw tolerance[4] and to enhance static fatigue limits.[30] It is the potential *degradation* of this same shielding that has important implications for fatigue.

Acknowledgments: We thank Y.-W. Mai for discussions, J. F. Kelly and D. E. Roberts for assistance with the experiments, and S. Derby for machining the specimens. Thanks are also due to J. Sibold of Coors Ceramics for providing the alumina.

References

[1]Y.-W. Mai and B. R. Lawn, "Crack Stability and Toughness Characteristics in Brittle Materials," *Annu. Rev. Mater. Sci.*, **16** 415–39 (1986).

[2]P. L. Swanson, C. J. Fairbanks, B. R. Lawn, Y.-W. Mai, and B. J. Hockey, "Crack-Interface Grain Bridging as a Fracture Resistance Mechanism in Ceramics: I, Experimental Study on Alumina," *J. Am. Ceram. Soc.*, **70** [4] 279–89 (1987).

[3]Y.-W. Mai and B. R. Lawn, "Crack-Interface Grain Bridging as a Fracture Resistance Mechanism in Ceramics: II, Theoretical Fracture Mechanics Model," *J. Am. Ceram. Soc.*, **70** [4] 289–94 (1987).

[4]S. J. Bennison and B. R. Lawn, "Role of Interfacial Grain-Bridging Sliding Friction in the Crack-Resistance and Strength Properties of Non-Transforming Ceramics," *Acta Metall.*, **37** [10] 2659–71 (1989).

[5]L. S. Williams, "Stress Endurance of Sintered Alumina," *Trans. Br. Ceram. Soc.*, **55** [5] 287–312 (1956).

[6]R. Sedlacek and F. A. Halden, "Static and Cyclic Fatigue of Alumina"; pp. 211–20 in *Structural Ceramics and Testing of Brittle Materials.* Edited by S. J. Acquaviva and S. A. Bortz. Gordon and Breach, New York, 1967.

[7]B. K. Sarkar and T. G. T. Glinn, "Fatigue Behavior of High Alumina Ceramics," *Trans. Br. Ceram. Soc.*, **69** [5] 199–203 (1970).

[8]D. A. Krohn and D. P. H. Hasselman, "Static and Cyclic Fatigue Behavior of a Polycrystalline Alumina," *J. Am. Ceram. Soc.*, **55** [4] 208–11 (1972).

[9]A. G. Evans and E. R. Fuller, "Crack Propagation in Ceramic Materials Under Cyclic Loading Conditions," *Metall. Trans.*, **5** [1] 27–33 (1974).

[10]S. Horibe and M. Sumita, "Fatigue Behavior of Sintered SiC; Temperature Dependence and Effect of Doping with Aluminum," *J. Mater. Sci.*, **23** [9] 3305–13 (1988).

[11]L. Ewart and S. Suresh, "Crack Propagation in Ceramics under Cyclic Loads," *J. Mater. Sci.*, **22** [4] 1173–92 (1987).

[12]M. J. Reece, F. Guiu, and M. F. R. Sammur, "Cyclic Fatigue Crack Propagation in Alumina under Direct Tension–Compression Loading," *J. Am. Ceram. Soc.*, **72** [2] 348–52 (1989).

[13]R. H. Dauskardt, W. Yu, and R. O. Ritchie, "Fatigue Crack Propagation in Transformation-Toughened Zirconia Ceramic," *J. Am. Ceram. Soc.*, **70** [10] C-248–C-252 (1987).

[14]R. H. Dauskardt, D. B. Marshall, and R. O. Ritchie, "Cyclic Fatigue Crack Propagation in Ceramics: Behavior in Overaged and Partially-Stabilized MgO–Zirconia"; in *Fracture Mechanics/Structural Ceramics.* Materials Research Society, Philadelphia, PA, in press.

[15]T. Kawakubo and K. Komeya, "Static and Cyclic Fatigue Behaviour of a Sintered Silicon Nitride at Room Temperature," *J. Am. Ceram. Soc.*, **70** [6] 400–405 (1987).

[16]M. Masuda, T. Soma, M. Matsui, and I. Oda, "Cyclic Fatigue of Sintered Silicon Nitride," *Ceram. Eng. Sci. Proc.*, **9** [9–10] 1371–82 (1988).

[17]M. Masuda, T. Soma, and M. Matsui, "Cyclic Fatigue Behaviour of Silicon Nitride Ceramics," *J. Eur. Ceram. Soc.*, **6** [4] 253–58 (1990).

[18]C.-W. Li, D. J. Lee, J. Yamanis, and I. Palley, "Cyclic Fatigue Properties of Silicon Nitride with Strong *R*-Curve Behavior"; presented at the 92nd Annual Meeting of the American Ceramic Society, Dallas, TX, 1990.

[19]J. T. Beals and I. Bar-On, "Fracture Toughness and Fatigue Crack Propagation of Silicon Nitride with Two Different Microstructures"; presented at the 14th Annual Conference on Composites and Advanced Ceramics, Cocoa Beach, FL, January 1990.

[20]C.-W. Li and J. Yamanis, "Super-Tough Silicon Nitride with *R*-curve Behavior," *Ceram. Eng. Sci. Proc.* **10** [7–8] 632–45 (1989).

[21]D. Lewis, "Cyclic Mechanical Fatigue in Ceramic–Ceramic Composites—An Update," *Ceram. Eng. Sci. Proc.*, **4** [9] 874–81 (1983).

[22]A. G. Evans, "Fatigue in Ceramics," *Int. J. Fract.*, **16** [6] 485–98 (1980).

[23]S. Suresh and J. R. Brockenbrough, "Theory and Experiments of Fracture in Cyclic Compression: Single-Phase Ceramics, Transforming Ceramics and Ceramic Composites," *Acta Metall.*, **35** [6] 1455–70 (1988).

[24]R. O. Ritchie, "Mechanisms of Fatigue Crack Propagation in Metals, Ceramics and Composites: Role of Crack Tip Shielding," *Mater. Sci. Eng.*, **A103**, 15–28 (1988).

[25]H. Frei and G. Grathwohl, "The Fracture Resistance of High Performance Ceramics by In Situ Experiments in the SEM" (in Ger.), *Beitr. Elektronenmikroskop. Direktabb. Oberfl.*, **22**, 71–78 (1989).

[26]S. Lathabai, Y.-W. Mai, and B. R. Lawn, "Cyclic Fatigue Behavior of an Alumina Ceramic with Crack-Resistance Curves," *J. Am. Ceram. Soc.*, **72** [9] 1760–63 (1989).

[27]J. Rödel, J. F. Kelly, and B. R. Lawn, "In Situ Measurements of Bridged Crack Interfaces in the SEM," *J. Am. Ceram. Soc.*, **73** [11] 3313–18 (1990).

[28]J. Rödel, J. F. Kelly, M. R. Stoudt, and S. J. Bennison, "A Loading Device for Fracture Testing of Compact Tension Specimens in the SEM," *Scanning Microsc.*, in press.

[29]D. B. Marshall, "An Improved Biaxial Flexure Test for Ceramics," *Am. Ceram. Soc. Bull.*, **59** [5] 551–53 (1980).

[30]S. Lathabai and B. R. Lawn, "Fatigue Limits in Noncyclic Loading of Ceramics with Crack-Resistance Curves," *J. Mater. Sci.*, **24** [12] 4298–306 (1989).

[31]*Annual Book of ASTM Standards,* Vol. 3.01, E-399-83. American Society for Testing and Materials, Philadelphia, PA, 1989.

[32]C. J. Beevers, K. Bell, R. L. Carlson, and E. A. Starke, "A Model for Fatigue Crack Closure," *Eng. Fract. Mech.*, **19** [1] 93–100 (1984).

[33]K.-T. Wan, S. Lathabai, and B. R. Lawn, "Crack Velocity Functions and Thresholds in Brittle Solids," *J. Eur. Ceram. Soc.*, **6** [4] 259–68 (1990).

[34]D. H. Buckley, *Surface Effects in Adhesion, Friction, Wear, and Lubrication;* Ch. 6. Elsevier, Amsterdam, Netherlands, 1981.

[35]X. Dong, S. Jahanmir, and S. M. Hsu, "Tribological Characteristics of α-Alumina at Elevated Temperatures," *J. Am. Ceram. Soc.*, **74** [5] 1036–44 (1991).

[36]D. B. Marshall and A. G. Evans, "Failure Mechanisms in Ceramic-Fiber/Ceramic-Matrix Composites," *J. Am. Ceram. Soc.*, **68** [5] 225–31 (1985). □